

Electronic Supplementary Material (ESI) for Journal of Materials Chemistry A

This journal is © The Royal Society of Chemistry 2018

**9.8%-efficient and above 100 h-stable unassisted solar water
splitting based on Si solar cells and photoelectrodes catalyzed by
bifunctional Ni-Mo/Ni**

Supporting Information

Ronglei Fan^{a,b}, Shaobo Cheng^c, Guanping Huang^a, Yongjie Wang^b, Yazhou Zhang^{b,d},
Srinivas Vanka^b, Gianluigi A. Botton^c, Zetian Mi^{b,*} and Mingrong Shen^{a,*}

^aSchool of Physical Science and Technology, Jiangsu Key Laboratory of Thin Films,
and Collaborative Innovation Center of Suzhou Nano Science and Technology,
Soochow University, 1 Shizi street, Suzhou 215006, China.

^bDepartment of Electrical Engineering and Computer Science, Center for Photonics and
Multiscale Nanomaterials, University of Michigan, 1301 Beal Avenue, Ann Arbor, MI
48109, United States.

^cDepartment of Materials Science and Engineering, Canadian Centre for Electron
Microscopy, McMaster University, 1280 Main Street West, Hamilton, Ontario,
L8S4M1, Canada.

^dInternational Research Center for Renewable Energy, Xi'an Jiaotong University, 28
West Xianning Road, Xi'an 710049, China.

***Corresponding Author**

Email: ztmi@umich.edu, Tel: 1 734 764 3963.

E-mail: mrshen@suda.edu.cn, Tel: 0086-0512-65112066.

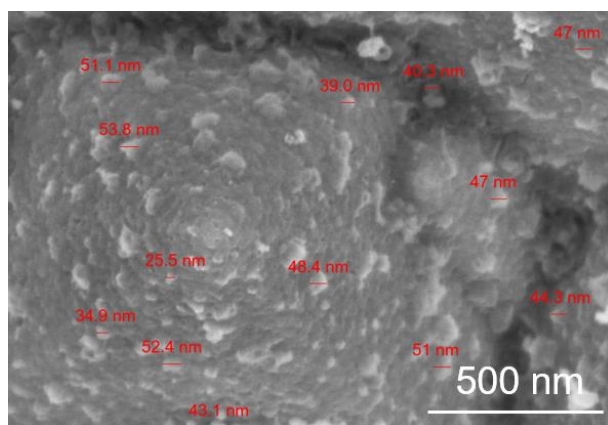


Fig. S1. Higher magnification surface SEM images of Ni-Mo/Ni/n⁺-Si, showing the mean size of Ni-Mo particles.

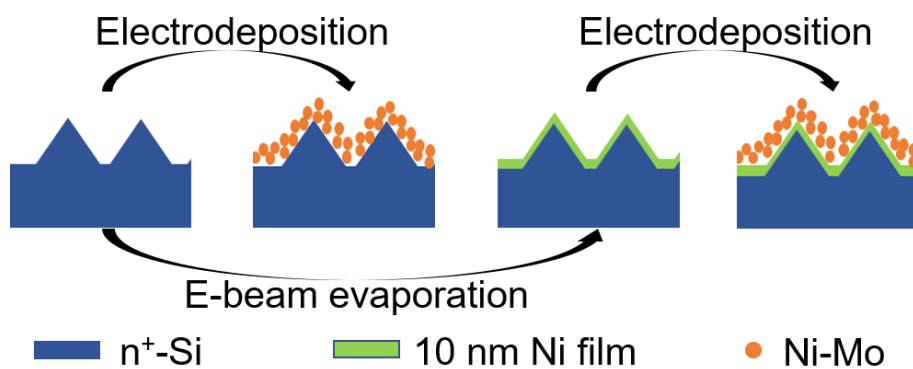


Fig. S2. Schematic representation of the fabrication procedures of Ni-Mo catalyst on n⁺-Si and Ni/n⁺-Si surfaces.

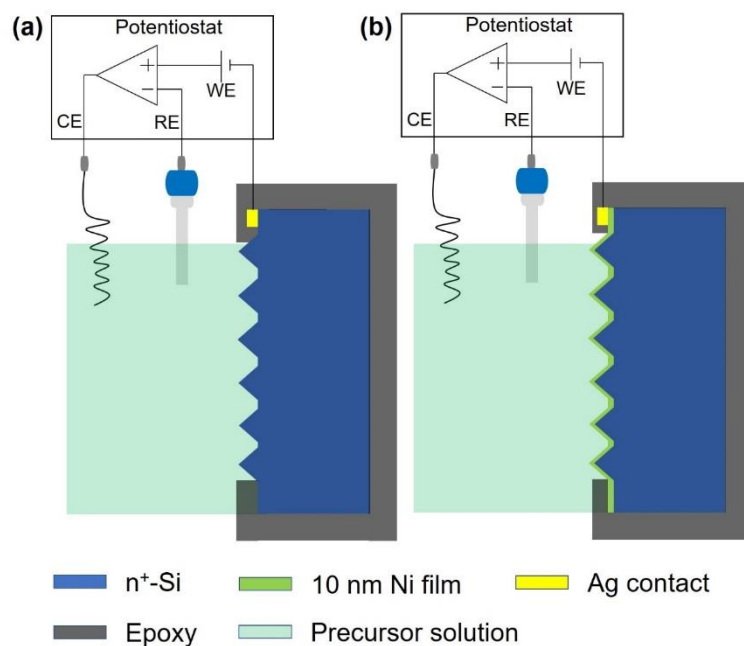


Fig. S3. Schematic overview of the electrodeposition setup of Ni-Mo catalyst for n^+ -Si and Ni/ n^+ -Si with micro-pyramid textured surface.

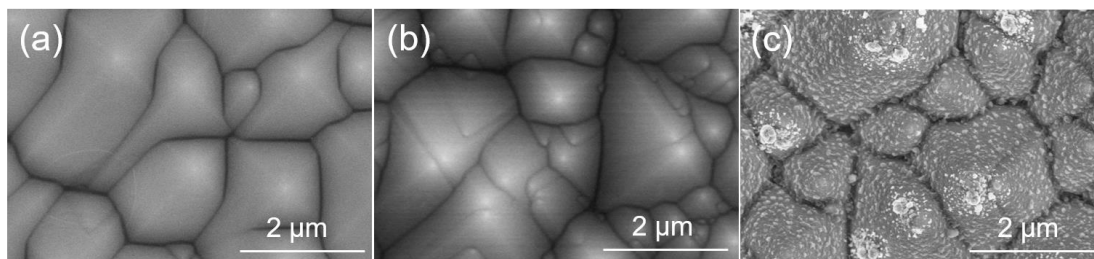


Fig. S4. Top-view SEM images of Ni/ n^+ -Si, n^+ -Si and Ni-Mo/ n^+ -Si.

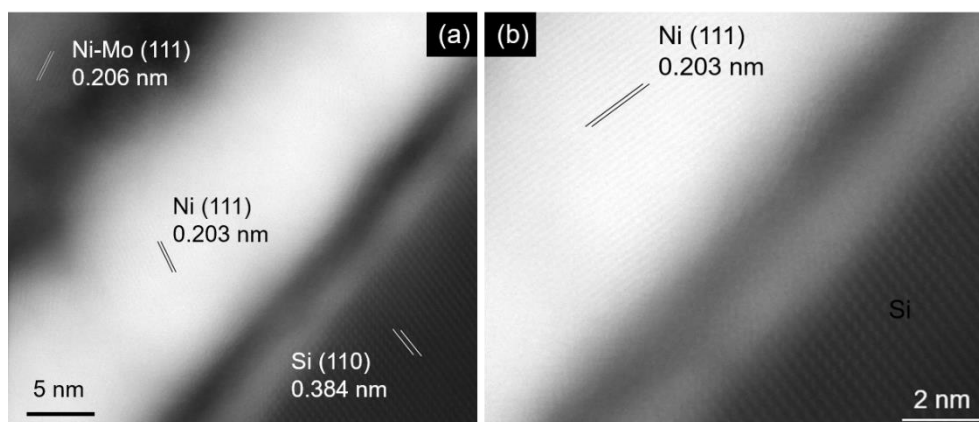


Fig. S5. Cross-sectional HR-TEM image of the as-synthesized Ni-Mo/Ni/ n^+ -Si electrode to show the interface of (a) Ni-Mo, Ni and Si and (b) Ni and Si more clearer.

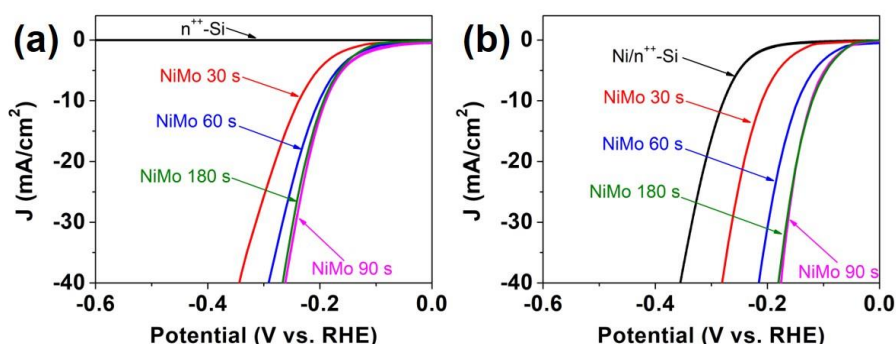


Fig. S6. LSV curves of Ni-Mo catalyst with various loading amount on (a) n^{++} -Si and (b) Ni/n^{++} -Si electrodes for HER. The amount of Ni-Mo catalyst on n^{++} -Si and Ni/n^{++} -Si electrodes was controlled by the deposition time of electrodeposition. The deposition time of 90 s exhibits the best HER electrocatalytic performance for both the n^{++} -Si and Ni/n^{++} -Si electrodes.

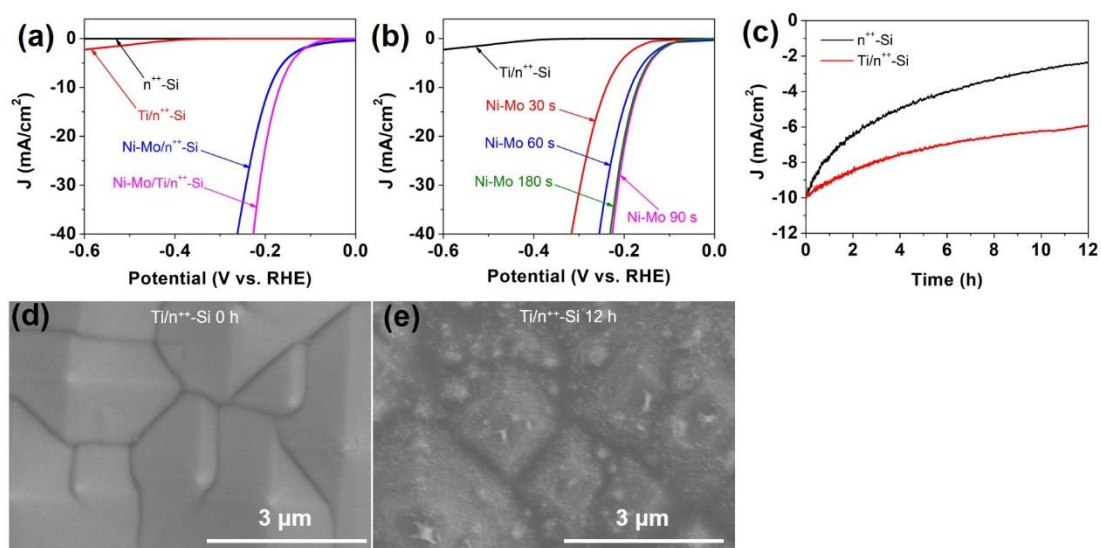


Fig. S7. Effect of the Ti buffer layer on HER electrocatalytic activities and long-term stability for n^{++} -Si and $Ni-Mo/n^{++}$ -Si electrodes in 1 M KOH. (a) LSV curves of n^{++} -Si electrodes with and without Ni-Mo catalyst layer and/or 10 nm Ti buffer layer. (b) LSV curves of Ni-Mo catalyst with various loading amount on Ti/n^{++} -Si electrodes. (c) Chronoamperometric $J-t$ test for n^{++} -Si and Ti/n^{++} -Si electrodes at a constant potential to achieve a current density of -10 mA/cm^2 for 12 h of continuous electrochemical H_2 evolution, respectively. Top-view SEM images of Ti/n^{++} -Si electrode (d) before and (e)

after 12 h of continuous electrochemical H₂ evolution.

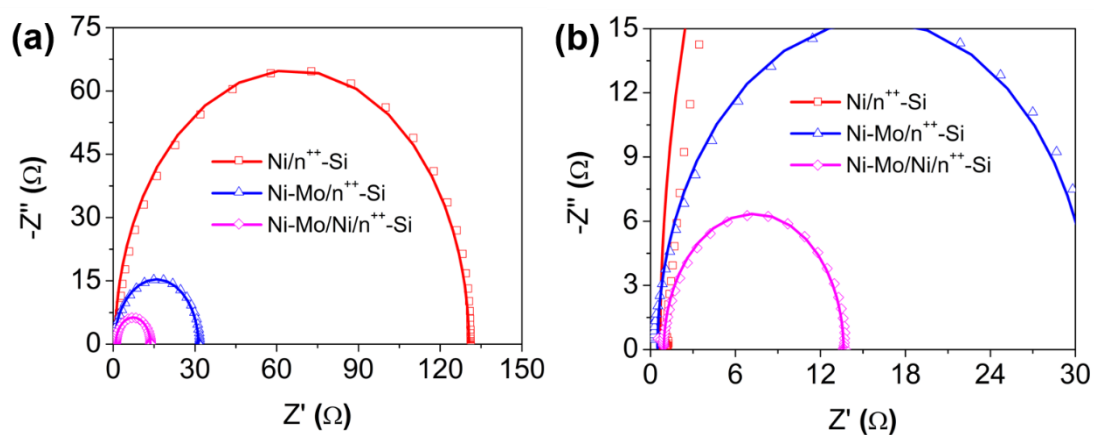


Fig. S8. (a) Nyquist plots for Ni, Ni-Mo and Ni-Mo/Ni catalysts on n⁺⁺-Si substrates at -0.1 V_{RHE} in 1 M KOH under AM 1.5G one sun illumination. (b) A detailed Nyquist plots for (a) at high frequency region.

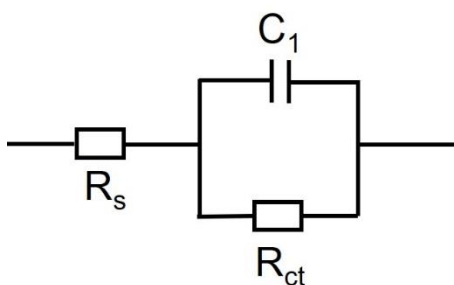


Fig. S9. The equivalent circuit model corresponding to the charge transfer from the n⁺⁺-Si to the electrolyte through a catalyst. The equivalent circuit elements include a series resistance (R_s) in series with a parallel arrangement of a resistor (R_{ct}) and a constant phase element (C_1).

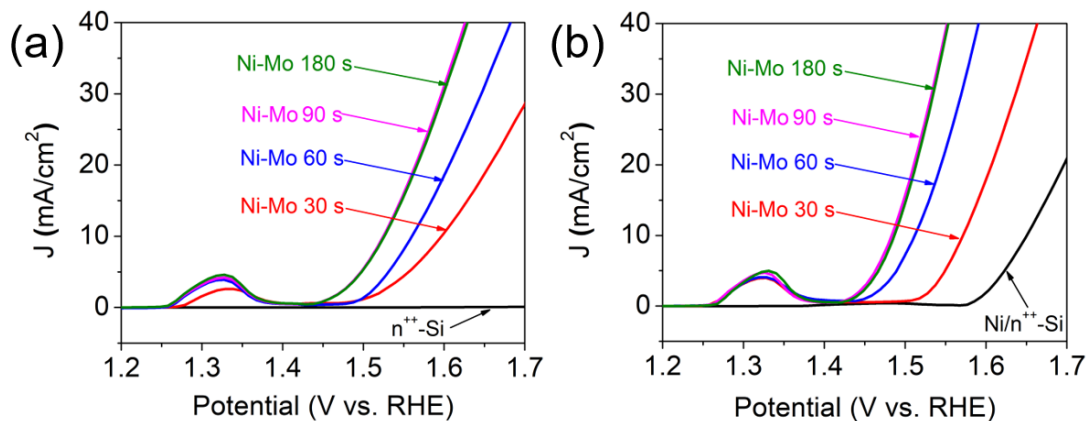


Fig. S10. LSV curves of Ni-Mo catalyst with various loading amount on (a) n^{++} -Si and (b) Ni/ n^{++} -Si electrodes for OER.

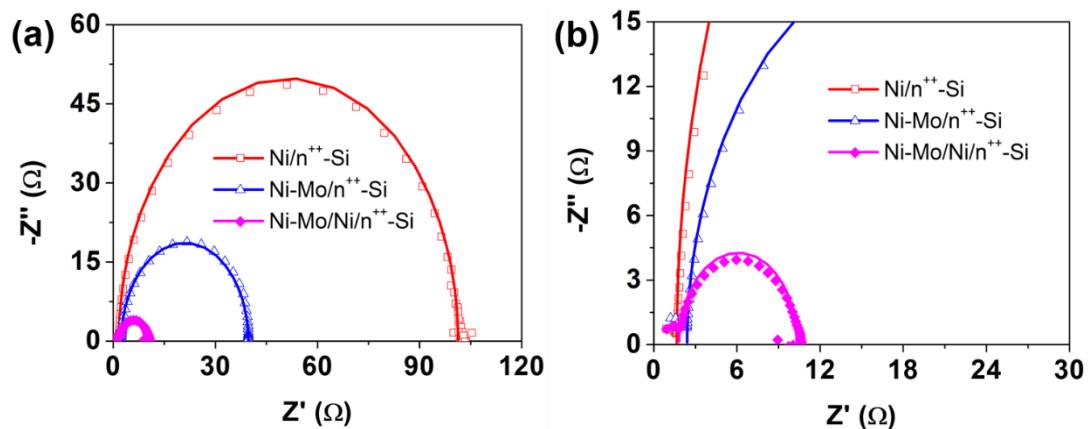


Fig. S11. (a) Nyquist plots for Ni, Ni-Mo and Ni-Mo/Ni catalysts on n^{++} -Si substrates at 1.3 V_{RHE} in 1 M KOH under AM 1.5G one sun illumination. (b) A detailed Nyquist plots for (a) at high frequency region.

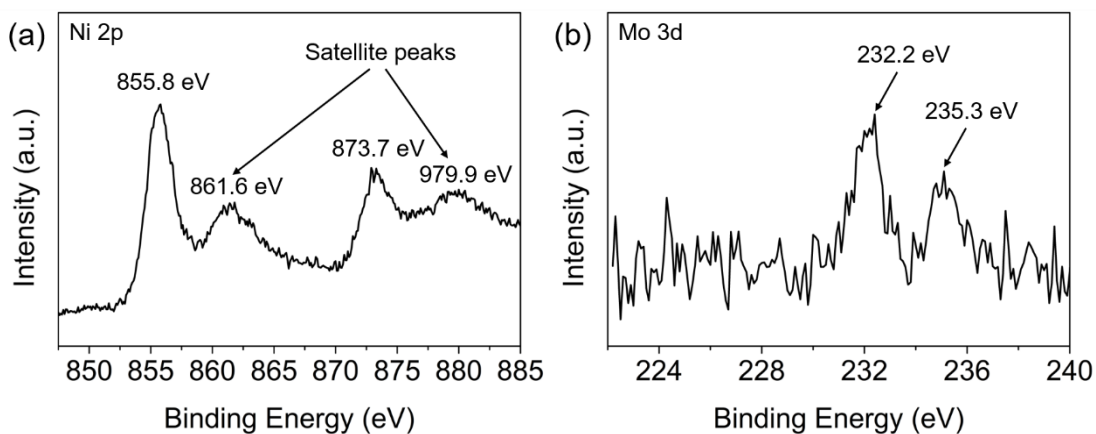


Fig. S12. High-resolution XPS spectra of (f) Ni 2p and (g) Mo 3d in Ni-Mo/Ni/n⁺⁺-Si electrode after 100 h continuous OER operation.

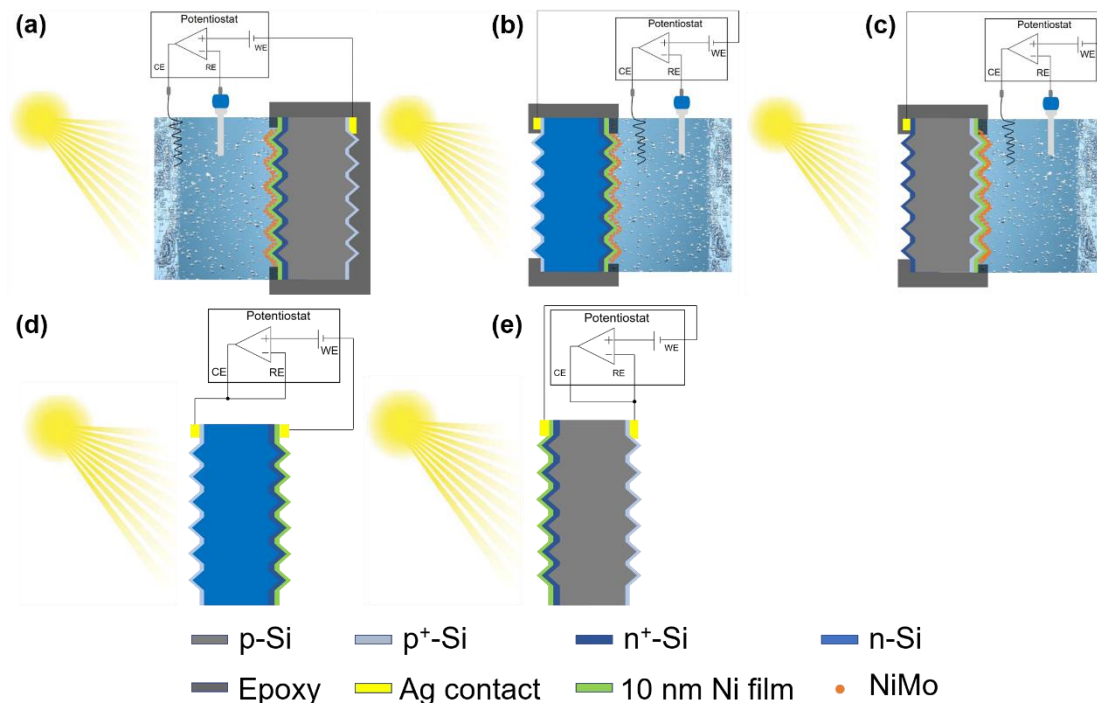


Fig. S13. (a) Schematic overview of the HER measurement setup for n⁺pp⁺-Si photocathodes. (b) Schematic overview of the HER measurement setup for n⁺np⁺-Si photocathodes. (c) Schematic overview of the OER measurement setup for p⁺pn⁺-Si photoanodes. (d) Schematic overview of the LSV measurement setup for n⁺np⁺-Si PV cells. (e) Schematic overview of the LSV measurement setup for n⁺pp⁺-Si PV cells.

Fig. S13 gives a schematic representation of how the potentiostat is connected to the samples to measure the PEC or PV performance of various samples. The samples are placed in the dark or under AM1.5 G 1 sun illumination (100 mW/cm²). CE is the counter electrode, RE is the reference electrode, and WE is the working electrode. Fig. S13d and e shows a schematic setup used to measure the LSV curves of the underlying PV cell. Note that the RE and CE are connected together at one side and that the WE is connected at the other side.

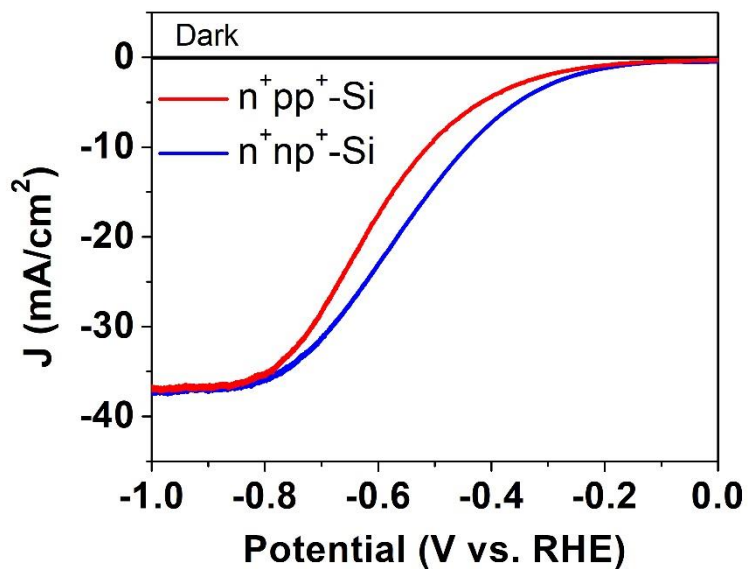


Fig. S14. LSV curves of bare n^+pp^+-Si and n^+np^+-Si photocathodes recorded in 1 M KOH solution (pH = 13.6) in the dark and under simulated AM1.5 G illumination (100 mW/cm²), respectively.

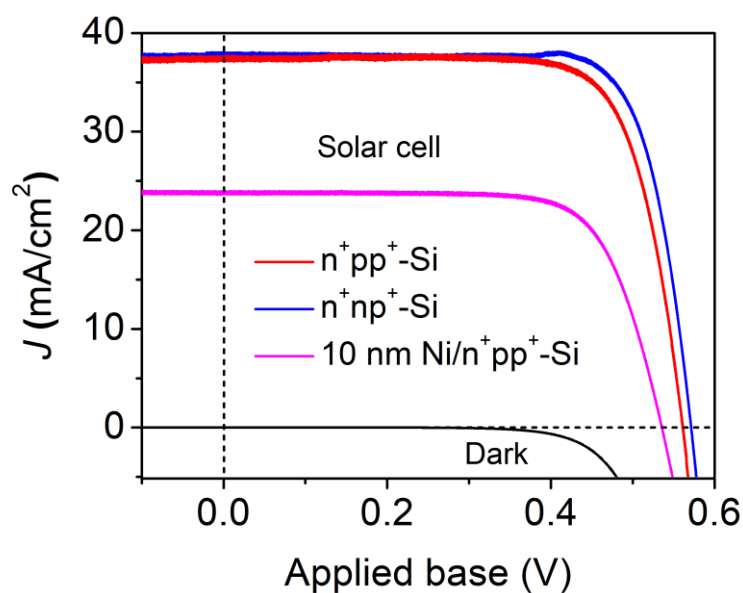


Fig. S15. LSV curves of bare n^+pp^+-Si , n^+np^+-Si and 10 nm Ni coated n^+pp^+-Si fabricated as solid-state Si PV cells.

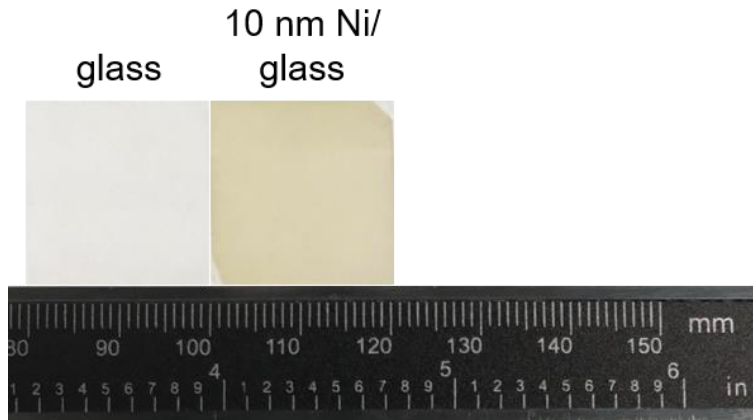


Fig. S16. Optical images of a transparent glass coated with and without 10 nm Ni.

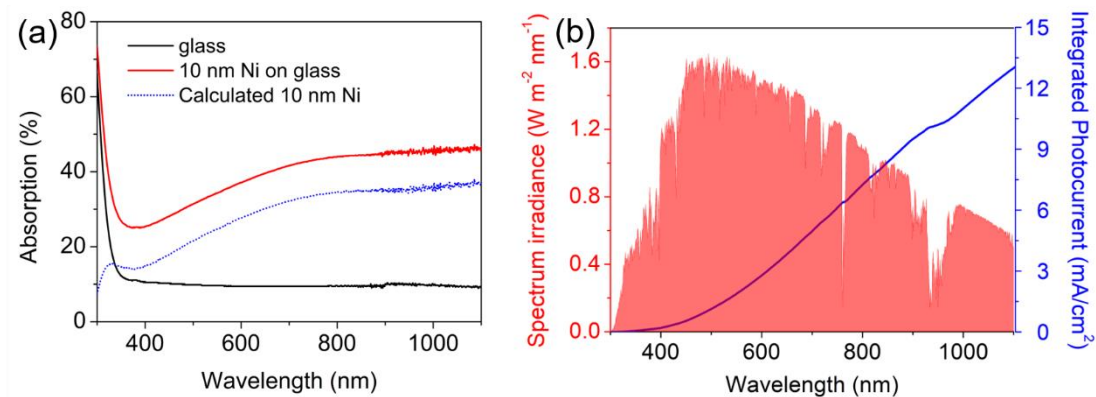


Fig. S17. (a) The UV–Vis absorption spectra of bare glass substrate, 10 nm Ni film on glass substrate and the calculated 10 nm Ni film, using a UV–vis–NIR spectrophotometer (UV-3600, Shimadzu). Considering the bandgap of Si (1.12 eV), the UV–Vis absorption spectra were conducted in the wavelength region of 300–1100 nm. (b) Integrated photocurrent density absorbed by 10 nm Ni film by integrating the absorption spectra in (a) with the standard solar spectrum of AM 1.5G (ASTM G173-03). An integrated photocurrent density of 13.0 mA/cm² (blue curve) was estimated, which is close to the difference in J_s (13.8 mA/cm²) between bare n⁺pp⁺-Si and 10 nm Ni coated n⁺pp⁺-Si measured in Fig. S15.

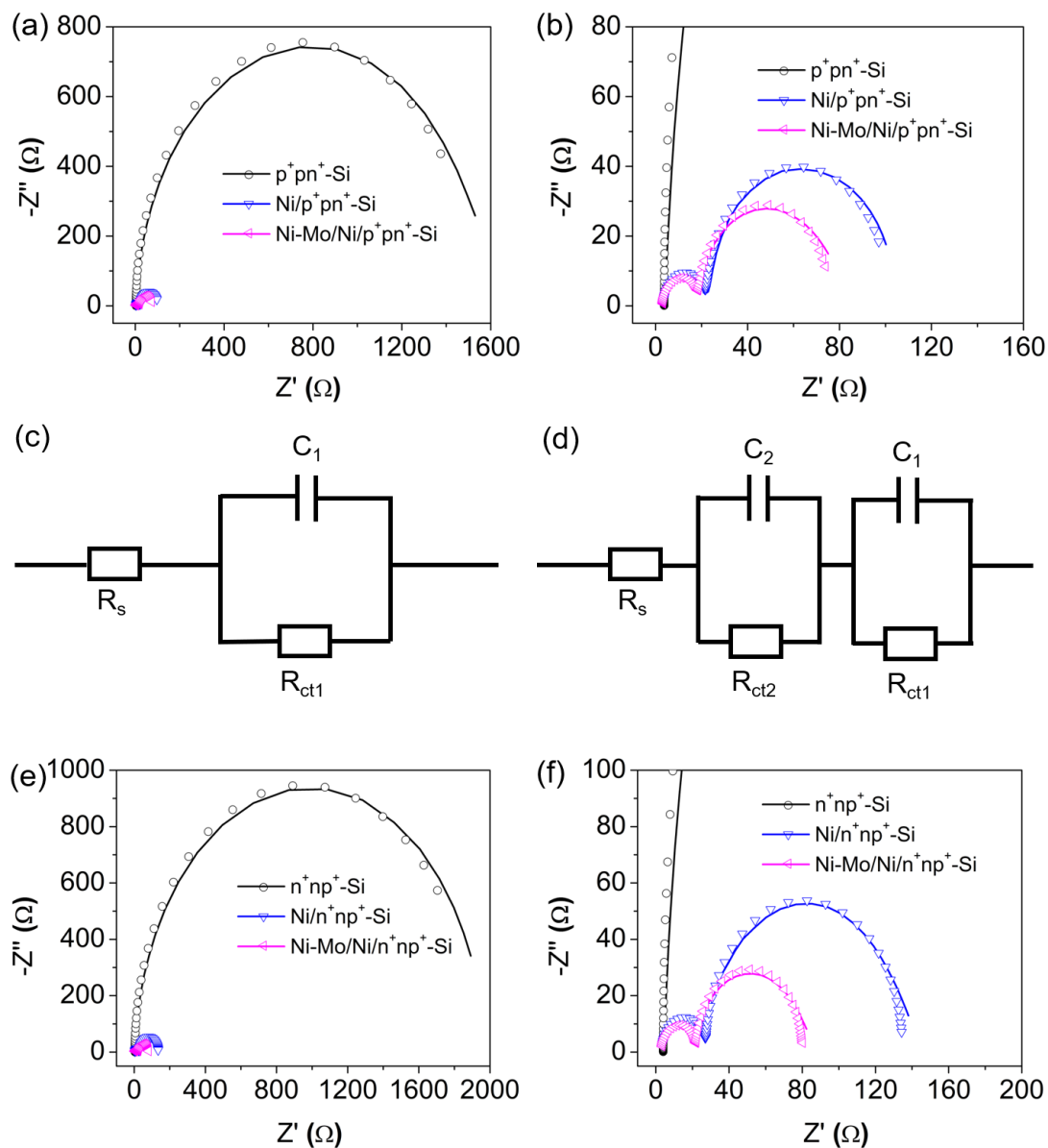


Fig. S18. (a) Nyquist plots of n^+np^+ -Si photocathodes with and without Ni and Ni-Mo/Ni catalyst measured at $-0.2 V_{RHE}$ under AM1.5G 1 sun illumination. (b) zoomed view of (a) to show the EIS spectra at small impedance region more clearly. The equivalent circuits for (c) pure n^+np^+ -Si photocathode and p^+pn^+ -Si photoanode, and for (d) n^+np^+ -Si photocathodes and p^+pn^+ -Si photoanode with Ni or Ni-Mo/Ni catalyst. (e) Nyquist plots of p^+pn^+ -Si photoanodes with and without Ni and Ni-Mo/Ni catalyst measured at $1.4 V_{RHE}$ under AM1.5G 1 sun illumination. (f) zoomed view of (e) to show the EIS spectra at small impedance region more clearly. The solid line traces correspond to the fitting using the corresponding equivalent circuit.

In (c), (d), R_s represents series resistance of the whole circuit. In (c), $R_{ct,1}$ represents the charge-transfer resistance from the Si photoelectrode to the electrolyte, and C_1 is the capacitance of the corresponding Si photoelectrode/electrolyte junction. In (d), $R_{ct,1}$ represents charge-transfer resistance from Si photoelectrode to Ni or Ni-Mo catalyst and C_1 is the capacitance of the corresponding Si photoelectrode/catalyst junction, $R_{ct,2}$ represents the charge-transfer resistance from the Ni or Ni-Mo catalyst to the electrolyte and C_2 is the capacitance of the corresponding catalyst/electrolyte junction.

The bare n^+np^+ -Si photocathodes displayed a large semicircle in the Nyquist plot (Fig. S18a), corresponding to the large resistance of direct charge transfer between the semiconductor Si and electrolyte. In contrast, the Ni/ n^+np^+ -Si and Ni-Mo/Ni/ n^+np^+ -Si photocathodes each exhibit two small semicircles. The one in high frequency range is related to the charge transfer in the interface of catalyst/Si and the other in low frequency range signifies the charge transfer of double layer at catalyst/electrolyte interface.

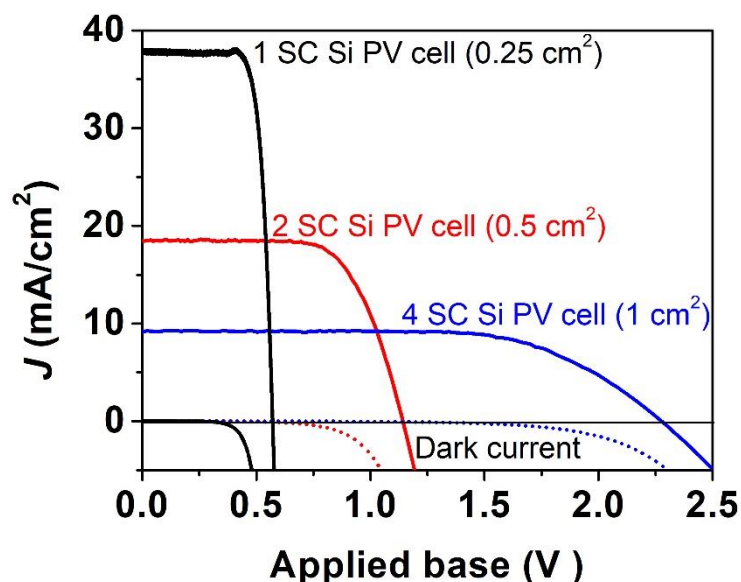


Fig. S19. LSV curves of SC Si PV cells under dark and AM1.5G 1 sun illumination. Black, red, and blue correspond to 1 cell (0.25 cm^2), 2 cells (0.5 cm^2), and 4 cells (1 cm^2), respectively.

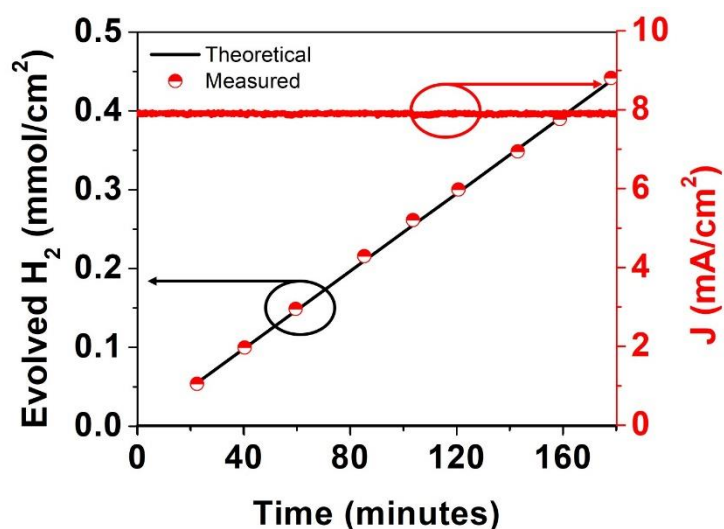


Fig. S20. Hydrogen gas evolution of the combined PV-PEC system was measured as a function of time at a zero bias in 1 M KOH under stimulated 1 sun AM 1.5G illumination.

The calculated H_2 production from photocurrent is also shown. The Faradaic efficiency (η_F) is obtained according the following equation:

$$\eta_F (\%) = \frac{2 \times \text{produced } H_2 (\text{mol} \cdot \text{cm}^{-2}) \times 96485 (\text{s} \cdot \text{A} \cdot \text{mol}^{-1})}{\text{photocurrent density } (\text{A} \cdot \text{cm}^{-2}) \times \text{time } (\text{s})} \times 100\%$$

The measured and theoretical hydrogen evolution agrees very well, confirming a nearly η_F of 100 % for the combined PV-PEC system.

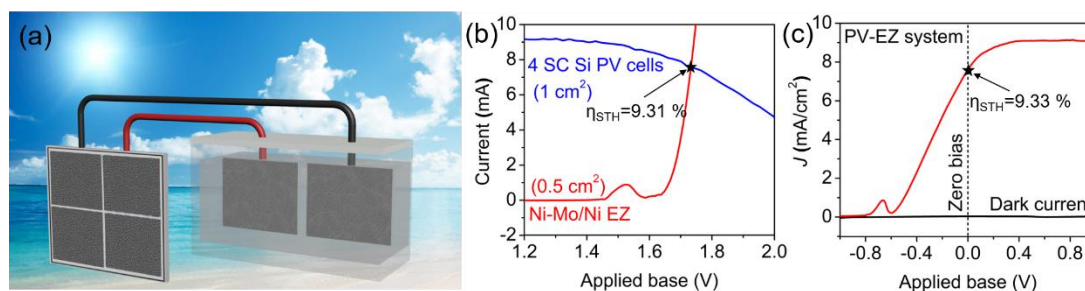


Fig. S21. Unassisted water splitting by using the combination of Ni-Mo/Ni electrolyzer and 4 SC Si PV cells. (a) Schematic illustration of the combined PV- EZ system. (b) Two-electrode LSV curves of the Ni-Mo/Ni electrolyzer under dark (red). Also shown are the LSV curves of 4 SC Si PV cells under AM1.5G 1 sun illumination (blue). Details of the 4 SC Si PV cells is shown in Fig. 17. Estimated η_{STH} for the combined PV-EZ

system is marked on the crossing point. (c) Two-electrode LSV curves of the combined PV-EZ system recorded in 1 M KOH under AM1.5G 1 sun illumination, showing the experimental η_{STH} .

Table S1. The corresponding Ni₄Mo electrocatalyst: XPS peak position, valence state and atomic ratio.

Peak	BE (eV)	Valence State	Atomic ratio (%)
Ni 2p _{1/2}	870.1	0	85
Ni 2p _{3/2}	852.8		
Mo 3d _{3/2}	231.2	0	15
Mo 3d _{5/2}	228.0		

Table S2. Characteristic parameters of the various photoelectrodes from the PEC LSV curves in Fig. 3.

	J_s (mA/cm ²)	J_0 (mA/cm ²)	V_o (V _{RHE})	η (%)
n ⁺ pp ⁺ -Si	-36.9	-0.2	-0.21	–
Ni/n ⁺ pp ⁺ -Si	-23.7	-13.7	0.21	0.60
Ni-Mo/Ni/n ⁺ pp ⁺ -Si	-21.1	-20.3	0.40	3.28
n ⁺ np ⁺ -Si	-37.1	-0.3	-0.18	–
Ni/n ⁺ np ⁺ -Si	-37.0	-30.2	0.29	2.17
Ni-Mo/Ni/n ⁺ np ⁺ -Si	-37.0	-36.3	0.50	6.90
Ni/p ⁺ pn ⁺ -Si	37.0	18.2	1.07	0.60
Ni-Mo/Ni/p ⁺ pn ⁺ -Si	37.0	34.5	0.94	3.11

Table S3. Summary of PEC performance of state-of-the-art Si photocathodes coated with earth-abundant catalysts.

	J_0 (mA/cm ²)	V_0 (V _{RHE})	ABPE (%)	Stability (h)	Electrolyte	Light intensity (mW cm ⁻²)	Ref.
Ni-Mo/Ni/n ⁺ np ⁺ - Si	-36.3	0.50	6.90	100	1 M KOH	100	This work
NiFe LDH/Ti/p-Si	-7	~0.3	< 0.5	24	1 M KOH	100	ACS Energy Lett. 2017, 2, 1939–1946
Ni/Ti/p-Si	-17	~0.3	< 0.5	12	1 M KOH	225	Nano Res. 2015, 8(5): 1577–1583
Si@CoSe ₂ MWs	-3.83	0.218	< 0.5	6	1 M KOH	100	ACS Appl. Mater. Interfaces 2016, 8, 5400–5407
NiO _x /SiO ₂ /p-Si	~-31	~0.8	~3.1	1	1 M KOH	100	ACS Appl. Mater. Interfaces 2018, 10, 7955–7962
Ni-Mo/NiSi/n ⁺ p- Si microwires	-29.8	0.55	10.1	288	1 M KOH	100	ACS Energy Lett. 2018, 3, 1086–1092
NiMo/n ⁺ p-Si	22.3	0.53	3.6	–	KHP, pH = 4.5	100	Energy Environ. Sci. 2012, 5, 9653- 9661
MoS ₂ /n ⁺ p-Si	17	0.32	< 2	100	0.5 M H ₂ SO ₄	100	Adv. Energy Mater. 2014, 1400739
MoS _x Cl _y /n ⁺ pp ⁺ -Si MPs	43	0.41	~6	2	0.5 M H ₂ SO ₄	100	Adv. Mater. 2015, 27, 6511–6518
CoPS/n ⁺ pp ⁺ -Si MPs	26	0.42	4.7	–	0.5 M H ₂ SO ₄	100	Nat. Mater. 2015, 14, 1245-1251
NiMo/TiO ₂ /n ⁺ p-Si microwire	14.3	0.42	2.9	7	0.5 M H ₂ SO ₄	100	Energy Environ. Sci. 2015, 8, 2977- 2984
MoS ₂ /Al ₂ O ₃ /n ⁺ p- Si	35.6	0.4	3.6	120	1 M HClO ₄	100	ACS Appl. Mater. Interfaces 2017, 9, 6123–6129
MoSe ₂ /n ⁺ p-Si	29.3	0.4	3.8	120	1 M HClO ₄	100	Appl. Phys. Lett. 2018, 112, 013902
Co-W-S/Ti/n ⁺ p-Si	-30.4	0.36	4.00	144	1 M HClO ₄	100	Appl. Catal. B: Environmental 237 (2018) 158–165

Table S4. Summary of PEC performance of state-of-the-art Si based photoanodes.

	J_0 (mA/cm ²)	V_o (V _{RHE})	ABPE (%)	Stability (h)	Electrolyte	Light intensity (mW cm ⁻²)	Ref.
Ni-Mo/Ni/p ⁺ np ⁺ - Si	37	0.94	3.11	100	1 M KOH	100	This work
FeNiCoO _x /TiO ₂ /G raphene/n-Si	~7	1	< 0.5	6	1 M KOH	100	Sustainable Energy Fuels, 2018, 2, 663–672
Ni/Pt/Al ₂ O ₃ /SiO _x / n-Si	19.2	0.997	~1	200	1 M KOH	100	Nature Commun. 2017, 8, 15968–
Ni ₈₀ Fe ₂₀ /TiO ₂ /n-Si	21.5	1.06	< 1	10	1 M KOH	100	ACS Catal. 2017, 7, 3277–3283
CoO _x /p ⁺ n-Si	30.8	~1	~1.5	72	1 M KOH	100	Nat. Mater. 2017, 16, 335–341
NiFe/SiO _x /np ⁺ -Si	30.7	0.89	3.3	13	1 M KOH	100	Adv. Energy Mater. 2016, 1601805
CoO _x /SiO _x /n-Si	23.2	1.02	1.42	2500	1 M KOH	100	Energy Environ. Sci. 2016, 9, 892–897
NiFe/NiCo ₂ O ₄ /np ⁺ -Si	> 25	0.95	~1.5	72	1 M KOH	100	J. Am. Chem. Soc. 2015, 137, 9595- 9603
NiO _x /CoO _x /SiO _x / n-Si	27.7	0.99	2.1	1700	1 M KOH	100	Energy Environ. Sci. 2015, 8, 2644-2649
NiO _x /np ⁺ -Si	29	1.05	2.1	1200	1 M KOH	100	J. Phys. Chem. Lett. 2015, 6, 592–598
Ni/TiO ₂ /np ⁺ -Si	11	1.08	< 0.5	110	1 M KOH	100	Science 2014, 344, 1005–1009
CoO _x /SiO _x /np ⁺ Si	17	~1.05	< 1	24	1 M KOH	100	J. Am. Chem. Soc. 2014, 136, 6191- 6194
IrO _x /Ir/p ⁺ n-Si	13.8	1.05	< 2	18	1 M H ₂ SO ₄	38.6 (λ> 635 nm, AM 1.5G)	J. Phys. Chem. Lett. 2014, 5, 1948- 1952
Fe-NiO/p ⁺ n-Si	17	~1.05	~2	300	1 M KOH	38.6 (λ> 635 nm, AM 1.5G)	J. Phys. Chem. Lett. 2014, 5, 3456- 3461

Table S5. The fitted value of charge transfer resistance and capacitance values for n^+np^+ -Si photocathodes and p^+pn^+ -Si photoanode with and without the Ni and Ni-Mo/Ni catalyst using the equivalent circuits listed in Fig. 16c and d.

Photoelectrodes	C_2 (F)	$R_{ct,2}$ (Ω)	C_1 (F)	$R_{ct,1}$ (Ω)	$R_{ct,1} + R_{ct,2}$ (Ω)
n^+np^+ -Si photocathode	—	—	2.3×10^{-5}	1510.1	1510.1
Ni/ n^+np^+ -Si photocathode	9.5×10^{-7}	19.1	5.9×10^{-5}	79.2	98.3
Ni-Mo/Ni/ n^+np^+ -Si photocathode	1.1×10^{-6}	16.3	1.5×10^{-4}	57.0	73.3
p^+pn^+ -Si photoanode	—	—	1.9×10^{-5}	1895.2	1895.2
Ni/ p^+pn^+ -Si photoanode	7.3×10^{-7}	24.6	6.7×10^{-5}	107.0	131.6
Ni-Mo/Ni/ p^+pn^+ -Si photoanode	9.4×10^{-7}	19.3	1.3×10^{-4}	58.2	77.5

Table S6. Summary of state-of-the-art unassisted solar water splitting based on PV–PEC configuration.

PV–PEC configuration	PV cells		η_{STH} (%)	Stability (h)	Ref.
	Efficiency (%)	Fill Factor			
2 SC Si PV cells–Ni–Mo/Ni/n ⁺ np ⁺ –Si and Ni–Mo/Ni/p ⁺ pn ⁺ –Si	14.3	0.684	9.8	105	This Work
2 SC c-Si PV cells–CoP/H/1% Mo:BiVO ₄ and CoP/Ni foam	13.27	–	5.3	2	J. Mater. Chem. A, 2018, 6, 1266–1274.
2 SC c-Si PV cells–BiVO ₄ and Fe ₂ O ₃	16.74	0.63	7.7	8	Nat. Comm. 2016, 7, 13380.
Perovskite cell–Fe(Ni)OOH/Mo:BiVO ₄	15.5	0.747	6.2	10	Sci. Adv. 2016; 2: e1501764
nc-Si:H/SHJ hybrid PV cell–Pt/TiO ₂ /a-SiC:H	10	0.701	7.9	–	Solar Energy Mater. Solar Cells, 2016, 150, 82-87.
Perovskite cell–Pt/TiO ₂ /ZnO/CdS/CuIn _x Ga _{1-x} Se ₂	~8	–	6.3	1	Adv. Energy Mater. 2015, 5, 1501520.
GaAs/InGaAsP/InP PV cell–Pt and Co-Pi/BiVO ₄ /WO ₃	~7	–	8.1	1	Sci. Rep. 2015, 5, 11141.
a-Si:H/nc-Si:H PV cell–Co-Pi/BiVO ₄ :W	9.6	0.624	5.2	–	ChemSusChem 2014, 7, 2832–2838.
3 junction a-Si PV cell–Ni and FeOOH/Mo:BiVO ₄	~14	–	2.5	12	Phys. Chem. Chem. Phys., 2014, 16, 15608-15614.
Double-junction a-Si PV cell–Co-Pi/BiVO ₄ :W	~10	–	4.9	1	Nat. Comm. 2013, 4, 2195.
Dye-sensitized PV cell–Pt/WO ₃	~6	–	3.1	9	Nat. Photonics 2012, 6, 824-828.

Table S7. Summary of state-of-the-art unassisted solar water splitting with Si-based PV–EZ configuration.

PV–EZ configuration	PV cells		η_{STH}	Stability (h)	Ref.
	Efficiency (%)	Fill Factor			
4 SC Si PV cells–Ni-Mo/Ni EZs	13.5	0.619	9.3	105	This work
3 SC Si PV cells–Ni-Co-S/Ni-Co-P EZ	14.4	0.621	10.8	48	J. Mater. Chem. A, 2018, 6, 20297-20303.
4 SC Si heterojunction PV cells–NiFe inverse opal EZs	14.49	0.593	9.54	25	Nano Energy 2017, 42, 1–7.
3 SC Si heterojunction PV cells–Pt and IrOx on Ni foam EZs	20.6	0.832	14.2	100	J. Electrochem. Soc., 2016, 163, F1177-F1181.
Pt/Ag/a-Si:H/a-Si:H–RuO ₂ EZ	9.9	0.778	6.8	50	Solar Energy Mater. Solar Cells, 2015, 140, 275–280.
Four single junction c-Si–NiBi and NiMoZn EZs	16	0.769	~9.7	168	Proc. Natl. Acad. Sci. U. S. A. 2014, 111, 14057-14061.
3 junction a-Si–Co-OEC and NiMoZn EZs	9	0.57	4.7	0.2	Science 2011, 334, 645-648.
4 Si PV arrays–Avalence high presure EZ	18.5	0.593	9.3	~372	Int. J. Hydrogen Energy 2008, 33, 2747-2764.